Combustion and Flame 231 (2021) 111492

Contents lists available at ScienceDirect

Combustion and Flame

journal homepage: www.elsevier.com/locate/combustflame

Connecting agglomeration and burn rate in a thermite reaction: Role of oxidizer morphology

Haiyang Wang[a], Dylan J. Kline[a,b], Prithwish Biswas[a], Michael R. Zachariah[a,*]

[a] Department of Chemical and Environmental Engineering, University of California, Riverside, CA 92521, United States
[b] Department of Chemical and Biomolecular Engineering, University of Maryland, College Park, MD 20742, United States

ARTICLE INFO

Article history:
Received 8 September 2020
Revised 26 April 2021
Accepted 27 April 2021

Keywords:
Imaging
Agglomeration
Propellants
Printing

ABSTRACT

Agglomeration (sintering) of aluminum particles has been commonly observed in solid propellants and pyrotechnics and it is believed to play a key role on the combustion performance of these materials. One of the most commonly studied nanothermites – Al/CuO – has also been well documented to exhibit this agglomeration phenomenon. In this work, high-speed *in-operando* microscopy and pyrometry were used to observe agglomeration in an Al/CuO reaction with different oxidizer particle size and shape (microparticles, microwires and nanoparticles). We found that the use of a microwire oxidizer resulted in propagation velocities and agglomerate sizes more similar to nanoparticles rather than microparticles. Replacing CuO microparticles (5 μm) with similarly-sized CuO microwires (equivalent diameter: 3 μm) was shown to dramatically elevate the burn rate by ~27 × (2 m/s vs 55 m/s) and increased the flame temperature from 2550 K to 3200 K, resulting in ~30 × higher heat flux (energy release rate). Adding 10 wt.% polymer into the above three thermite systems slowed down the burn rates from ~m/s to ~cm/s, which allowed our microscopic system to probe the details of the agglomeration process. The agglomeration size was found to be reduced from ~40 μm to ~13 μm when replacing CuO microparticles with microwires in the 3D printed Al/CuO composites, similar to that of CuO nanoparticles case. Our results point to a "pocket" model to explain these trends. In a reactive composite, CuO microwires should create an Al "pocket" closer in size to that when using CuO NPs and considerably smaller that with CuO microparticles. The reduced pocket size should also enhance burn velocity. These results also suggest the "pocket" offers a pathway to think about architectures to minimize the sintering size which is known to lead to two-phase losses in propellants.

1. Introduction

Aluminum (Al) particles are commonly used in energetic materials include propellants, explosives and pyrotechnics to increase the overall energy density of the composite [1–4]. When replacing the conventional aluminum microparticles with nano-sized counterparts, energy release rate can be promoted with lower ignition thresholds [5–7]. However, the nano-sized Al particles pose unique processing problems [8–10] and also experience agglomeration (sintering) issues during combustion [11–13]. This sintering process not only hinders overall energy release from the metal fuel, but also leads to significant deviations from the implied faster energy release rate since the actual size of the particles burning are the larger agglomerates rather than the original micro- or nanoparticles [11–13]. Agglomeration of aluminum (Al) particles has been commonly observed in solid propellants, which lead to losses in specific impulse (two-phase loss) and ultimately balances out any potential advantages of Al addition [14–16]. Using capture/quench studies, the agglomerate size of Al has been related to the burn rate of solid propellants and various approaches have been explored to efficiently reduce the effect of sintering [17–19]. In addition to ex-situ studies, recently developed techniques such as time-resolved X-ray imaging [20,21] and digital in-line holography [15,16] have been employed to observe these processes *in-situ*.

Thermites are a class of energetic materials whose reactivity can be systematically adjusted by changing chemistry (e.g. stoichiometry, reactant choice), particle size, mixing state, and architecture/morphology. Changes in chemical composition can be employed to manipulate the reaction mechanism as a means to modulate performance, while the latter variables are more related to physical effects such as heat transfer and interfacial surface area. However, these factors are inherently entangled since the heat transfer rates can impact reaction rate and vice versa, mak-

* Corresponding author.
E-mail address: mrz@engr.ucr.edu (M.R. Zachariah).

https://doi.org/10.1016/j.combustflame.2021.111492
0010-2180/

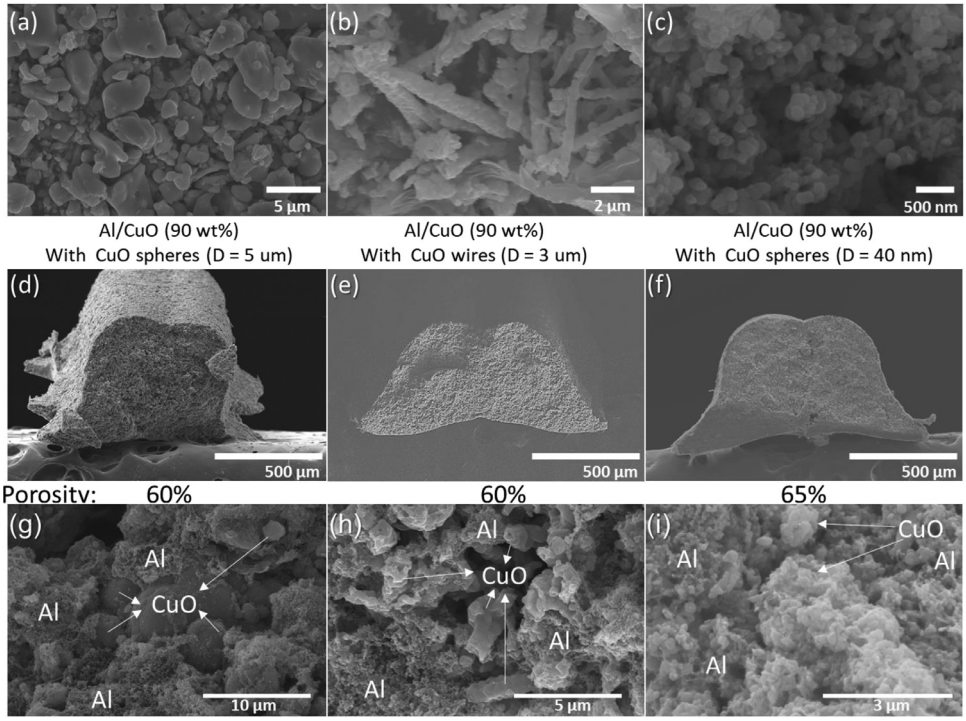

Fig. 1. Cross-sectional SEM image of 3D printed high loading (90 wt%) sticks (d-f) with CuO microspheres (~5 µm, a), wires (equivalent diameter ~3 µm, b) and nanospheres (~80 nm, c). Higher resolution SEM images of 3D printed high loading (90 wt%) sticks (g-i).

ing it difficult to independently probe these effects. High-speed imaging is quite useful in assessing various combustion regimes as it is the most direct method to interrogate the complexity of such heterogeneous systems during reaction [19–25]. Due to the higher flame temperature and burn rate of nanothermites compared to solid propellants, it is difficult to probe the reaction in a high spatial and temporal resolution. More recently, high-speed microscopy and pyrometry has been found to be a useful technique to observe the propagation of printed nanothermites on a glass slide [22–25] at high spatial (µm) and temporal (µs) resolution. These studies indicate the significance of the agglomeration (sintering) of Al on the corrugation of the flame front. However, due to the high burn rate (~m/s) and thin reaction front (~2–3 µm), the rapid Al agglomeration was not clearly imaged.

In this work, a polymer mixture (10 wt.%) is used to print free-standing sticks of Al/CuO nanothermites, which significantly slows down the chemistry from m/s to cm/s and enables us to directly observe the agglomeration in the thermite reaction at a spatial and temporal resolution of ~µm and ~µs, respectively. When replacing CuO microparticles with CuO microwires, we find reactivity is commensurate with CuO nanoparticles. We explore the role of oxidizer particle size and shape (microparticles, microwires and nanoparticles) on the agglomeration process with *in-operando* high-speed microscopy/pyrometry and demonstrate the correlation between agglomeration size/ejection speed and the flame propagation speed. We find that our results are very consistent with a "pocket" model, where in the CuO encapsulates a region of Al that confines the final sintering size of Al. The smaller the pocket, the faster the burn and the lower the expected two-phase losses.

2. Experimental data

2.1. Materials and printing

CuO microwires (Fig. 1b) were prepared by oxidizing Cu wires (purchased from US Research Nanomaterials) in air at 500 °C for 4 h (Figure S1). Al NPs (80 wt.% active, 81 nm), CuO microparticles (~5 µm, Fig. 1a), and CuO nanoparticles (~40 nm, Fig. 1c) were purchased from Novacentrix Inc, Sigma-Aldrich and US Research Nanomaterials, respectively. METHOCEL^{TM} F4M Hydroxypropyl Methylcellulose (HPMC) and polyvinylidene fluoride (PVDF, average molecular weight: ~534,000) were obtained from Dow Chemical Company and Sigma-Aldrich, respectively and were mixed and used as the hybrid polymer binder.

For 100 wt.% case, Al and a stoichiometric amount of CuO particles were dispersed in ethanol (250 mg/mL) by ultrasonication for ~1 hour and then printed on glass slides (22 mm × 22 mm, 1 mm thick) placed along the printing route (bed temperature~40 °C). The low- and high-magnifications SEM images of the printed pure thermite films are shown in Figure S2. Free-standing composite sticks (90 wt.% Al/CuO) were 3D-printed by a previously published method [6]. When preparing the ink, HPMC and PVDF were dissolved in DMF, followed by addition of the stoichiometric CuO and Al NPs, and then the mixture was magnetically and mechanically stirred to obtain homogenization. The slurry ink was printed (16-gage nozzle) into lines on a pre-heated substrate (~75 °C) and cut into 3 cm long sticks. The porosity of sticks (90 wt.% active) were calculated as ~ (1-actual density/theoretical density) based on at least 5 sticks [23]. The low- and high-resolution SEM images of the printed free-standing sticks (90 wt.% thermite loading) are shown in Fig. 1d-f and g-i, respectively. The typical formulation is shown in Table S1.

2.2. Macroscopic and microscopic imaging

The experimental system used in this study is shown in Fig. 2. The samples are either powder films deposited on glass slides at 100 wt.% (~2.2 cm long, ~4 mm wide, and ~ 150 µm thick) or free-standing burn sticks (~3 cm long, ~1 mm wide, and ~1 mm thick) with 90 wt.% reactive particulate material. For the sticks, we had only a front-view, while for the deposited powders on slides we imaged both from the front and side-view (cross-sectional).

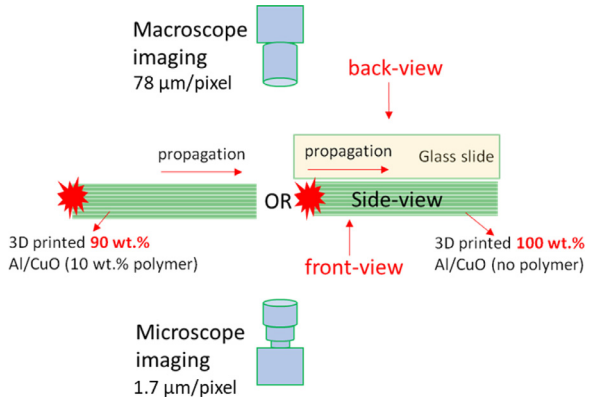

Fig. 2. Schematic showing the experimental setup used in this study.

Samples were placed between two camera systems with different resolutions triggered simultaneously to get two videos for a single event. On one side of the film, a macroscopic imaging high-speed camera (Vision Research Phantom Miro M110) captures the back side at a sample rate of 7000 frames/s, while the other side consists of a high-speed microscope imaging system (Vision Research Phantom VEO710L coupled to Infinity Photo-Optical Model K2 DistaMax) which captures the front side at a sample rate of 60,000 frames per second (resolution: ~1.7 μm/pixel, capturing area: 512 × 512 pixels). Typical optical images from microscopic system were shown in Figure S3.

The burn rate and flame temperature were obtained from the macroscopic imaging system since it can resolve the entire combustion event without having to focus on a small area. The details of color pyrometry can be found in previous studies [24]. Briefly, three channel intensity (red, green, blue) ratios are extracted to obtain the reaction flame temperature as calibrated with a blackbody source (Mikron M390). Raw videos are processed using a house-built MATLAB routine and demosaiced for the camera's Bayer filter using the built-in MATLAB algorithms, and the corresponding flame temperature maps were output and reported. The threshold errors for data acceptance and false colorization temperature assignment in the experiments for this work were set nominally to ~200–300 K. The post-combustion products were characterized by a NNS450 scanning electron microscope (SEM) and Energy Dispersive X-ray Spectroscopy (EDX) (ThermoFisher Scientific, formerly FEI/Philips).

3. Results

Three different CuO oxidizers were explored in this study with 100% and 90% thermite loadings: ~5 μm diameter microparticles (CuO MPs), ~15 μm (length) × 1 μm (diameter) microwires (CuO MWs), ~40 nm diameter nanoparticles (CuO NPs) (Fig. 1). In particular, the CuO MWs have a calculated equivalent spherical volume diameter of ~3 μm, so the CuO MWs and CuO MPs are roughly the same volume. Nevertheless, the calculated specific surface area (per mass) varies widely and can be ranked as CuO NPs (125) >> CuO MWs (7) > CuO MPs (normalized to 1). The CuO MWs actually have nano-sized structures as observed in the SEM (Fig. 1b) which may mean they have a higher specific surface area than calculated. Considering that CuO NPs agglomerate (up to μm as shown in Fig. 1i), their interfacial surface area will be significantly lower than the estimated specific surface area.

3.1. 100% printed powder films

To directly demonstrate the effects of CuO size and morphology on thermite propagation, we 3D-printed Al/CuO ink on a glass slide to form a thin thermite film without using any binder (cross-sectional SEM images are in Figure S2). The thermite film is very brittle but could hold its integrity during testing. We were not able to measure the absolute densities of these pure thermite films, but we estimated them relative density to be 1 (CuO MPs), ~0.83 (CuO MWs) and ~1.07 (CuO NPs), based on their thicknesses (weight and width/length is the same). We measured the average burn rates (Fig. 3) as well as the flame temperatures of Al/CuO composite films (no polymers) on a glass slide (thickness: ~1 mm) (Figure S4-S6 and Table 1). With CuO MWs and NPs, the films burn at an average speed of ~55 m/s and ~33 m/s, respectively, which is >15x higher than that of Al/CuO with CuO MPs (~2 m/s). Moreover, the flame temperatures (Table 1 and Figure S4-S6) of CuO MW- and NP-based thermites are measured as ~3000–3200 K, respectively, which is ~500 K higher than that of the CuO MPs case (~2550 K). The normalized heat flux normalized (Table 1) is in the order of CuO NPs (21) ≈ CuO MWs (29) >> CuO MPs (normalized to 1), which further reinforces the impressive performance of the CuO MWs based thermites. It is noted that when it is 100 wt.% thermite loading, the burn rates and heat flux of the microwire case is even higher than that of nanoparticle case, which might be due to its relatively lower density and enhancement in convective heat transfer.

Table 1
Burning rate, flame temperature and normalized heat flux of different Al/CuO composite with 100 wt.% and 90 wt.% thermite loading.

Al/CuO composites		Burn rate (cm/s)	Flame temp. (K)	Relative densities	Normalized heat flux
100 wt.%	Microparticles	200	2550	1.00	1.00
	Microwires	5500	3200	0.83	29.00
	Nanoparticles	3300	3000	1.07	21.00
90 wt.%	Microparticles	2.20	2050	1.00	1.00
	Microwires	2.60	2220	1.00	1.28
	Nanoparticles	2.94	2710	0.88	1.56

Interestingly and unexpectedly, both the CuO MWs and NPs based thermites could be ignited at ~<970 K according to a fast-heating (~10^5 K/s) wire ignition method [23], which is 200 K lower compared to the CuO MPs case (~1170 K) (Figure S7). Though one might find the ignition temperature differences correlate to those of the burn rates, we reserve a more detailed exploration of this phenomenon for future studies.

In this study, the comparative reactivity between the CuO MW- and NP-based thermites is the most surprising considering the CuO MWs case has a volume ~100x larger than the CuO NPs. To probe how agglomeration/sintering during combustion may be relevant in this observation, we employed microscopic imaging on the propagation of these Al NP-based thermites in addition to the conventional macroscopic imaging (Fig. 2). We observed *in-operando* how the agglomeration droplets were formed and propagated to the neighboring unburnt area (Fig. 4 and Figure S8-S12). The ignition points propagate radially at a speed of ~1.4 m/s and ~1.0 m/s for CuO MW- and NP-based thermites, respectively, which is 5–7 times higher than the CuO MPs case (Fig. 4 and Figure S8-S12). The key takeaway from this section is to reinforce our observation that oxidizer microwires behave much more like nanoparticles rather than microparticles.

Though our camera successfully captured the whole process of agglomeration (coalescing, bubbling and micro-explosion, Fig. 4 and details in Figure S12) for Al/CuO with CuO MPs case, for the Al/CuO with CuO MWs and NPs cases, the propagation is so fast that we could only obtain a few snapshots of the event (Fig. 4). To explore this observation further, it was necessary to slow down the propagation to a level more suitable for imaging with our high-speed microscopy apparatus.

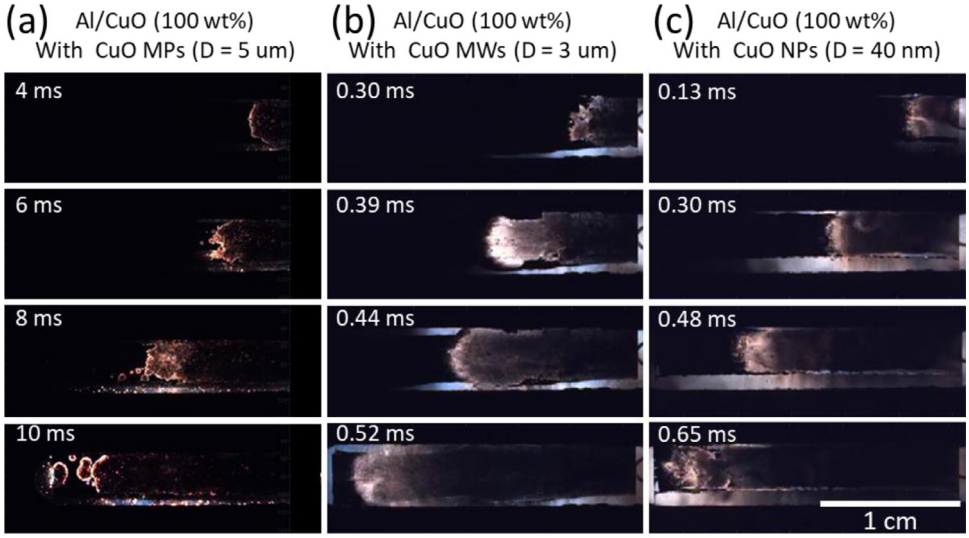

Fig. 3. Typical propagation snapshots of 3D printed Al/CuO composites with 100 wt.% particle loading (no polymers) with CuO MPs (a), MWs (b) and NPs (c) in macroscopic scale.

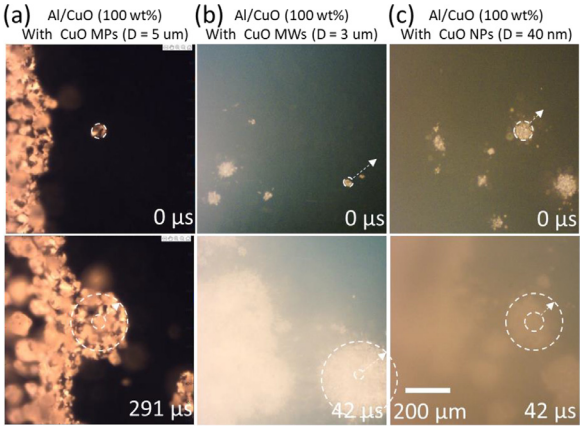

Fig. 4. Typical snapshots of how agglomeration ejections igniting and propagating.

3.2. Free-standing sticks (90 wt.% thermite loading)

To slow down propagation to a level amenable to image agglomeration effects, we added a 10 wt.% polymer mixture into our nanothermite formula and, using our previously reported technique [23], directly wrote free-standing nanothermite sticks. This resulted in a significant reduction of the macroscopic burning rate from ~m/s to ~cm/s, which is in its own right an interesting topic for study (possible explanations in supporting). However, for the purposes of this paper, we have chosen to focus on the slower burning nanothermite sticks since the burn rate reduction produced higher fidelity data with our imaging apparatus.

We begin with the microscopic burning images of the CuO MPs-based thermite (90 wt.% Al/CuO sticks). The reaction front shows the formation of large, highly emissive, molten droplets (2100–2800 K) formed on the surface (dash lines) of the composite sticks (Fig. 5a). The temperature of these spheres is significantly higher than the melting point of Al (melting point, MP: 933 K) and CuO (MP: 1600 K) and the formation of spheres confirms they are molten. These droplet spheres continually grow in size from the coalescence of smaller droplets driven by surface tension before lifting off from the burning surface (Fig. 5a-c). The lifting off only occurs when the Al_2O_3 cap is observed in the droplets and the temperature approaches ~2400 K (Al_2O_3 melting point) [14–19]. The process of coalescence is rapid (<~0.1 ms) and consistent with the time scale we have observed previously [25].

The same basic processes appear to be taking place for the CuO MWs and NPs cases (See Fig. 5b, c respectively). However, differences in particle size are obvious in the images and are quantified in the size distribution histograms shown in Fig. 5a-1~5c-1. In both the CuO MW and NP cases, the droplet sizes are much smaller compared to the CuO MP case (~15 µm vs ~40 µm). Consistent with the coalescing size in Fig. 5, the post-combustion residues shown in Figure S13 clearly indicate that the residue size of CuO MP case is ~5–10 times larger than that of CuO MWs and NPs.

Fig. 5 also shows that the molten droplets in the cases of the CuO MWs and NPs (~1.2 m/s) are ejected with higher velocity than the CuO MP case (~0.4 m/s) (details in supporting). The differences in molten droplets velocities suggests higher gas generation rates, and thus faster reaction, and are consistent with the macroscopic flame propagation results. As shown in Fig. 5d, the burn rate and flame temperature ranked as CuO NPs > CuO MWs > CuO MPs. The higher temperature for the nanomaterial is not surprising as it suggests more complete combustion. Normalized heat flux estimations (= burn rate × flame temperature × density) also follow the same trend CuO NPs (1.56) > CuO MWs (1.28) > CuO MPs (1, as baseline) as summarized in Table 1.

4. Discussion

In summary, we see that the MWs have a behavior closer to that of the NPs over that of the MPs in both microscopic and macroscopic scales. We must now ask why microwires produce such small droplets in comparison to microparticles. Obviously, there are many complex phenomena involved, but one possible explanation is inspired by the “pocket model” theory where the volume of the agglomerated particles produced is predominately controlled by the effective volume of Al particles that can be aggregated within a surrounding oxidizer matrix (depicted in Fig. 6) [26–28].

Herein, we construct a simple model of the pocket size of the three different Al/CuO composites with CuO MPs, MWs and NPs. The “pocket” of Al NPs is assumed to be a cube whose size is determined by the density and size of the different CuO morphologies employed, which constrains the “pocket”. The “pocket size”, (a_{Al}), is the length of the cube (pocket). As shown in Fig. 6a, to estimate the size of the pocket in the three cases, the volume (Vol.)

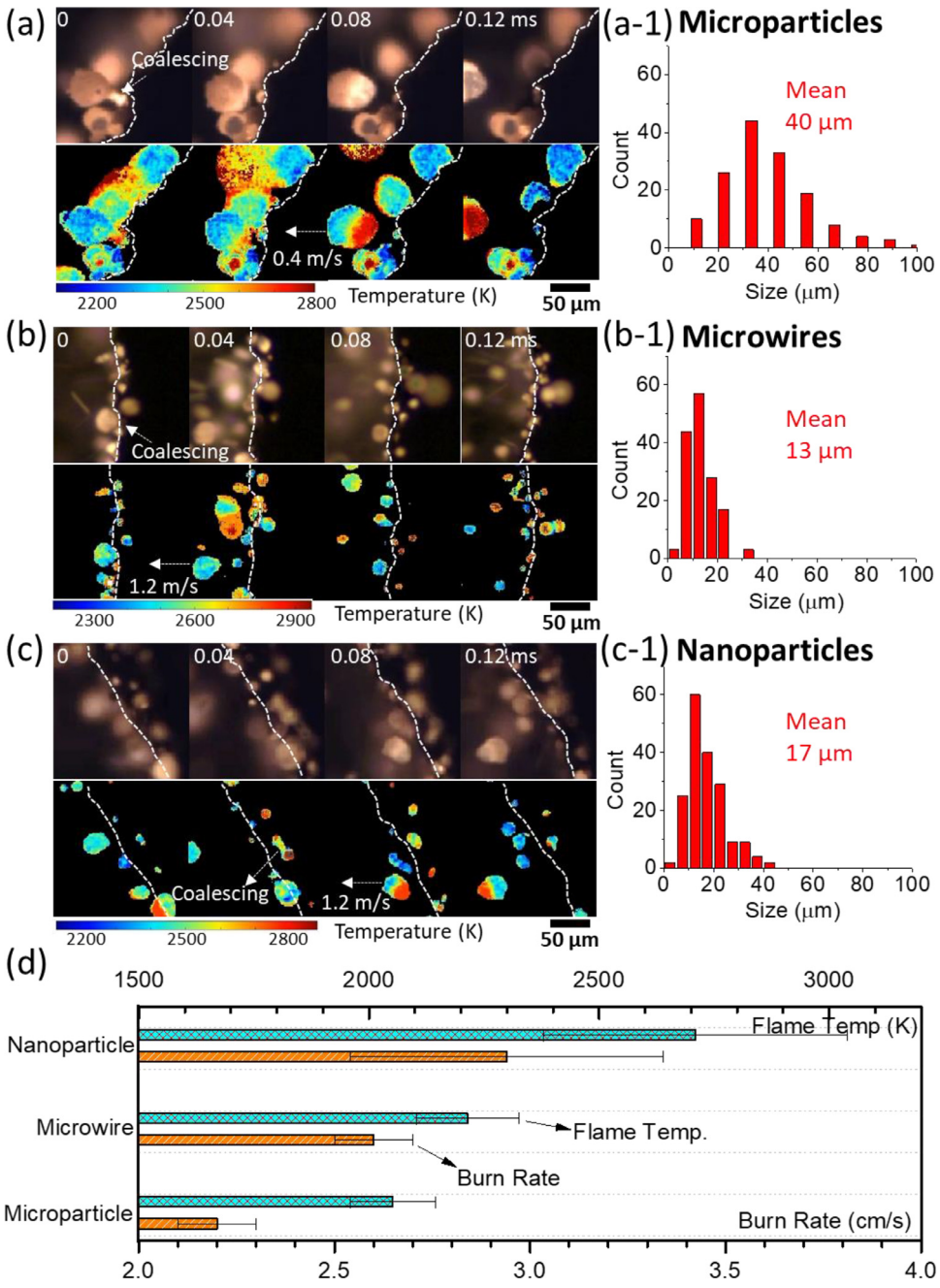

Fig. 5. The evolution of agglomerations (a-c) with different size distributions (a-1~c-1) observed in the microscopic burning surface of Al/CuO composite sticks (90 wt.%) with CuO microparticles (a), microwires (b) and nanoparticles (c). Full images could be found in Figure S14-S17 and supporting videos. The sizes of the agglomerations were measured and averaged based on >150 agglomeration droplets in the high-speed videos. Summary of burning rate and flame temperature (d, details in Figure S18). Δt is ~42 μs between two neighbor frames.

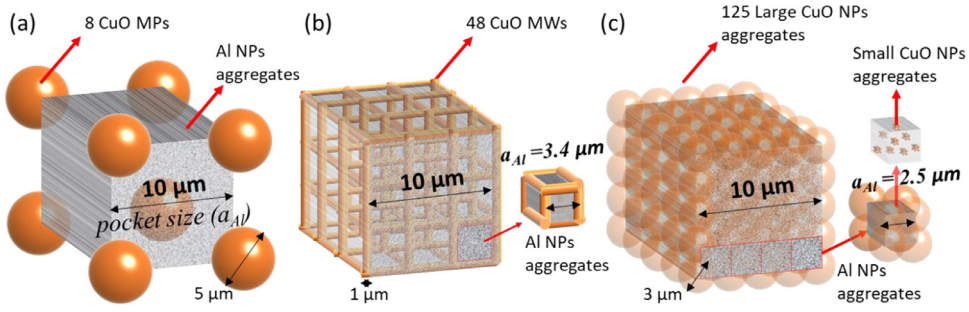

Fig. 6. Schematic illustrating the "pockets" of Al in Al/CuO composites with different CuO morphologies - MPs (diameter 5 μm), MWs (diameter 1 μm, length 15 μm) and NPs (diameter 3 μm). The resulting pocket size of different composites is labeled as ~10 μm, ~3.4 μm and ~2.5 μm.

Table 2
Pocket size calculation results.

	CuO MPs	CuO MWs	CuO NPs
$Vol._{Al}/Vol._{CuO}$	1.95	1.95	0.65
Φ_{CuO} (μm)	5.00	2.82	3.00
Pocket size: a_{Al} (μm)	10.1	3.4	2.5
Sintered size: Φ_{Al} (μm)	8.8	2.9	2.2
Measured Φ_{Al} (μm)	40	13	17
Measured / Calculated	4.6	4.5	7.9

ratio of Al to CuO was used. To account for the known lower packing density of fractal aggregates, the volume of Al and CuO NPs aggregates was increased 3× [29]. For Al/CuO with CuO microparticles and microwires, the Al/CuO volume ratio is 1.95 based on Equation (S2) and 0.65 for Al/CuO with CuO nanoparticles based on Equation (S3).

As we noted in the experimental section, the volume-based equivalent diameter (Φ_{CuO}) of CuO MPs and MWs is ~5 μm and 2.8 μm, respectively. The original size of CuO NPs is ~40 nm and the aggregate size of CuO NPs was estimated as ~3 μm based on SEM observations (Fig. 1). Assuming a cubic control volume of 10 μm sides, we will have 8 CuO MPs (8 corners in the cube), 48 CuO MWs (4 × 4 × 3) and 125 CuO NPs (5 × 5 × 5) for this superlattice to construct the structure in Fig. 6. The size of the smallest confined pocket unit (a_{Al}) of Al NPs in CuO MPs, CuO MWs, and CuO NPs is ~10 μm, ~3.4 μm and ~2.5 μm, respectively (Fig. 6).

As schematically shown in Fig. 6 and numerically in Table 2, the high aspect ratio of CuO MWs results in ~1/30 smaller pocket volume (a_{Al}^3) than the CuO MP's. The point being that the smaller pocket limits the effective size of the Al aggregate that can be formed during combustion [30]. If we assume that the pocket operates independently due to the gas generation of CuO (which can break apart sintered aggregates), we can estimate the size of the resulting sintered Al particle since we know that the packing density of Al fractal aggregates in the pocket is ~35% [23,29]. Based on this, the diameter of the average Al sintering size (Φ_{Al}) from the corresponding "pocket" can be calculated as 8.8 μm, 2.9 μm, and 2.2 μm for MPs, MWs, and NPs, respectively ($\Phi_{Al} = 0.874 a_{Al}$).

This result indicates that the microwires should yield Al sintered particles that are about the same size as those generated from composites made with CuO NPs, and about factor of three smaller than those formed during reactions with CuO MPs. This is qualitatively consistent with the experimental observation (see histograms in Fig. 5). Our calculated particles sizes are smaller than measured, however this is expected since the assumption of independent pockets is a gross approximation. Nevertheless, the trends are clear and unambiguous.

5. Conclusions

In this work, high-speed microscopy and pyrometry on a ~μm space and ~μs time scale were used to observe agglomeration from Al/CuO thermite combustion with different oxidizer particle size and shape (microparticles, microwires, and nanoparticles). We found that the use of CuO microwires rather than microparticles makes the propagation velocity and the extent of agglomeration behave like CuO NPs. In fact, replacing CuO microparticles (5 μm) with similarly-sized CuO microwires (equivalent diameter: 3 μm) was shown to dramatically elevate the burn rate by ~ 27 × (2 m/s vs 55 m/s) and increase the flame temperature from 2550 K to 3200 K, resulting in ~30 × higher heat flux (energy release rate). Adding 10 wt.% polymer into the above three thermite systems slows down the burn rates from ~m/s to ~cm/s, which allows our microscopic system to probe the details of the agglomeration process. The agglomeration size in the microscopic burning of the 3D printed Al/CuO composites was found to be reduced from ~40 μm to ~13 μm when replacing microparticles with microwires. A simple mechanism based on the "pocket model" was employed to explain why CuO microwires based thermite produces small agglomeration and high energy release rate. This study might provide new approaches to reduce the Al agglomerations and reduce two-phase loss in solid rocket propulsion.

Declaration of Competing Interest

None.

Acknowledgments

The authors gratefully acknowledge support from the Air Force Office of Scientific Research. Electron microscopy on quenched samples was performed using a FEI NNS450 SEM in the Central Facility for Advanced Microscopy and Microanalysis at University of California, Riverside.

Supporting information

SEM of different CuO, the corresponding 3D printed composites (90 wt.% Al/CuO loading sticks and 100 wt.% Al/CuO loading films) and post-combustion residues. Experimental setup, microscopic and macroscopic snapshots/videos, and summarized data including burn rates, flame temperature, and heat flux of different samples.

Supplementary materials

Supplementary material associated with this article can be found, in the online version, at doi:10.1016/j.combustflame.2021.111492.

References

[1] R.A. Yetter, Progress towards nanoengineered energetic materials, Proc. Combust. Inst. (2020) In press.
[2] E.L. Dreizin, Metal-based reactive nanomaterials, Prog. Energy Combust. Sci. 35 (2019) 141–167.
[3] L.T. DeLuca, Overview of Al-based nanoenergetic ingredients for solid rocket propulsion, Def. Technol. 14 (2018) 357–365.
[4] X. Ma, Y. Li, I. Hussain, R. Shen, G. Yang, K. Zhang, Core–shell structured nanoenergetic materials: preparation and fundamental properties, Adv. Mater. 32 (2020) 2001291.
[5] D. Sundaram, V. Yang, R.A. Yetter, Metal-based nanoenergetic materials: synthesis, properties, and applications, Prog. Energy Combust. Sci. 61 (2017) 293–365.
[6] M. Comet, C. Martin, F. Schnell, D. Spitzer, Nanothermites: a short review. Factsheet for experimenters, present and future challenges, Propellants Explos. Pyrotech. 44 (2019) 18–36.
[7] J.J. Granier, M.L. Pantoya, Laser ignition of nanocomposite thermites, Combust. Flame. 138 (2004) 373–383.
[8] L.U. Meda, G. Marra, L. Galfetti, F. Severini, L. De Luca, Nano-aluminum as energetic material for rocket propellants, Mater. Sci. Eng. C 27 (2007) 1393–1396.
[9] J. Zhi, L. Shu-Fen, Z. Feng-Qi, L. Zi-Ru, Y. Cui-Mei, L. Yang, L. Shang-Wen, Research on the combustion properties of propellants with low content of nano metal powders, Propellants Explos. Pyrotech 31 (2006) 139–147.
[10] D. Wen, Nanofuel as a potential secondary energy carrier, Energy Environ. Sci. 3 (2010) 591–600.
[11] L. Galfetti, L.T. DeLuca, F. Severini, G. Colombo, L. Meda, G. Marra, Pre and post-burning analysis of nano-aluminized solid rocket propellants, Aerosp. Sci. Technol. 11 (2007) 26–32.
[12] E.A. Lebedeva, I.L. Tutubalina, V.A. Val'tsifer, V.N. Strel'nikov, S.A. Astaf'eva, I.V. Beketov, Agglomeration of the condensed phase of energetic condensed systems containing modified aluminum, Combust. Explos. Shock Waves 48 (2012) 694–698.
[13] P. Chakraborty, M.R. Zachariah, Do nanoenergetic particles remain nano-sized during combustion? Combust. Flame 161 (2014) 1408–1416.
[14] W. Ao, X. Liu, H. Rezaiguia, H. Liu, Z. Wang, P. Liu, Aluminum agglomeration involving the second mergence of agglomerates on the solid propellants burning surface: experiments and modeling, Acta Astronaut. 136 (2017) 219–229.

[15] Y. Chen, D.R. Guildenbecher, K.N. Hoffmeister, M.A. Cooper, H.L. Stauffacher, M.S. Oliver, E.B. Washburn, Study of aluminum particle combustion in solid propellant plumes using digital in-line holography and imaging pyrometry, Combust. Flame 182 (2017) 225–237.
[16] B. Jin, Z. Wang, G. Xu, W. Ao, P.J. Liu, Three-dimensional spatial distributions of agglomerated particles on and near the burning surface of aluminized solid propellant using morphological digital in-line holography, Aerosp. Sci. Technol. (2020) 106066.
[17] K. Tejasvi, V.R. Vemana, P.S. Yelamarthi, J. Kandasamy, Ultra-fine aluminum characterization and its agglomeration features in solid propellant combustion for various quenched distance and pressure, Propellants Explos. Pyrotech. 45 (2020) 714–723.
[18] L. Li, X. Chen, C. Zhou, W. Li, M. Zhu, Experimental and model investigation on agglomeration of aluminized fuel-rich propellant in solid fuel ramjet, Combust. Flame 219 (2020) 437–448.
[19] W. Ao, P. Liu, H. Liu, S. Wu, B. Tao, X. Huang, L.K.B. Li, Tuning the agglomeration and combustion characteristics of aluminized propellants via a new functionalized fluoropolymer, Chem. Eng. J. 382 (2020) 122987.
[20] E.R. Wainwright, S.V. Lakshman, A.F.T. Leong, A.H. Kinsey, J.D. Gibbins, S.Q. Arlington, T. Sun, K. Fezzaa, T.C. Hufnagel, T.P. Weihs, Viewing internal bubbling and microexplosions in combusting metal particles via x-ray phase contrast imaging, Combust. Flame 213 (2019) 194–203.
[21] M.D. Grapes, R.V. Reeves, K. Fezzaa, T. Sun, J.M. Densmore, K.T. Sullivan, In situ observations of reacting Al/Fe2O3 thermite: relating dynamic particle size to macroscopic burn time, Combust. Flame 201 (2019) 252–263.
[22] H. Wang, B. Julien, D.J. Kline, Z. Alibay, M.C. Rehwoldt, C. Rossi, M.R. Zachariah, Probing the reaction front of nanolaminates at ~μs time and ~μm spatial resolution, J. Phys. Chem. C 124 (2020) 13679–13687.
[23] H. Wang, J. Shen, D.J. Kline, N. Eckman, N.R. Agrawal, T. Wu, P. Wang, M.R. Zachariah, Direct writing of a 90 wt% particle loading nanothermite, Adv. Mater. 23 (2019) 1806575.
[24] D.J. Kline, Z. Alibay, M.C. Rehwoldt, A. Idrogo-Lam, S.G. Hamilton, P. Biswas, F. Xu, M.R. Zachariah, Experimental observation of the heat transfer mechanisms that drive propagation in additively manufactured energetic materials, Combust. Flame (2020) 417–424.
[25] H. Wang, D.J. Kline, M.R. Zachariah, In-operando high-speed microscopy and thermometry of reaction propagation and sintering in a nanocomposite, Nat. Commun. 10 (2019) 1–8.
[26] N.S. Cohen, A pocket model for aluminum agglomeration in composite propellants, AIAA J. 21 (1983) 720–725.
[27] F. Maggi, L.T. DeLuca, A. Bandera, Pocket model for aluminum agglomeration based on propellant microstructure, AIAA J. 53 (2015) 3395–3403.
[28] J.K. Sambamurthi, E.W. Price, R.K. Sigman, Aluminum agglomeration in solid-propellant combustion, AIAA J. 22 (1984) 1132–1138.
[29] C. Zangmeister, J. Radney, L.T. Dockery, J.T. Young, X. Ma, R. You, M.R. Zachariah, The packing density of rigid aggregrates is independent of scale, PNAS 111 (2014) 9037.
[30] L.A. Povinelli, Effect of Oxidizer Particle Size On Additive agglomeration, NASA Technical Note D-1438, 1962.